ACS APPLIED MATERIALS & INTERFACES

Research Article

www.acsami.org

Improved Efficiency of Inverted Organic Light-Emitting Diodes Using Tin Dioxide Nanoparticles as an Electron Injection Layer

Hyunkoo Lee,[†,§] Chan-Mo Kang,[†] Myeongjin Park,[†] Jeonghun Kwak,*[,‡] and Changhee Lee*[,†]

[†]Department of Electrical and Computer Engineering, Inter-university Semiconductor Research Center, Seoul National University, Seoul 151-744, Republic of Korea

[‡]Department of Electronic Engineering, Dong-A University, Busan 604-714, Republic of Korea

Supporting Information

ABSTRACT: We demonstrated highly efficient inverted bottom-emission organic light-emitting diodes (IBOLEDs) using tin dioxide (SnO_2) nanoparticles (NPs) as an electron injection layer at the interface between the indium tin oxide (ITO) cathode and the organic electron transport layer. The SnO_2 NP layer can facilitate the electron injection since the conduction band energy level of SnO_2 NPs (−3.6 eV) is located between the work function of ITO (4.8 eV) and the lowest unoccupied molecular orbital (LUMO) energy level of typical electron transporting molecules (−2.5 to −3.5 eV). As a result, the IBOLEDs with the SnO_2 NPs exhibited a decrease of the driving voltage by 7 V at 1000 cd/m^2 compared to the device without SnO_2 NPs. They also showed a significantly enhanced luminous current efficiency of 51.1 cd/A (corresponds to the external quantum efficiency of 15.6%) at the same brightness, which is about two times higher values than that of the device without SnO_2 NPs. We also measured the angular dependence of irradiance and electroluminescence (EL) spectra in the devices with SnO_2 NPs and found that they had a nearly Lambertian emission profile and few shift in EL spectrum through the entire viewing angles, which are considered as remarkable and essential results for the application of OLEDs to display devices.

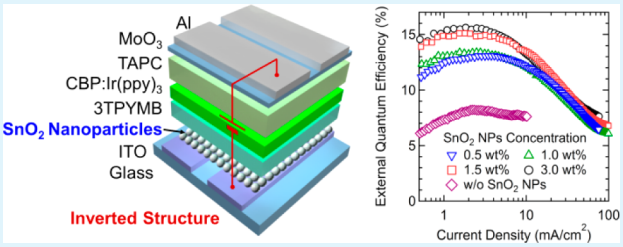

KEYWORDS: *organic light-emitting diodes, inverted structure, tin dioxide nanoparticles, interfacial layers, electron injection layer, metal oxide*

INTRODUCTION

In recent years, the organic light-emitting diodes (OLEDs) have attracted much scientific and commercial interest for full-color displays and lighting sources owing to the advantages of their flexibility, low power-consumption, high color purity and contrast, and many others.[1−3] The active-matrix (AM) OLEDs are already utilized in the commercial products such as portable multimedia players, mobile phones, and digital cameras. However, there are many technological obstacles to making larger display panels with low costs in AMOLEDs, and the compatibility with the thin film transistor (TFT) backplane is one of them. So far, most of the commercialized AMOLED panels have used the low temperature poly silicon (LTPS) TFT backplane because of its high mobility, stability, and availability of the p-type transistor characteristics, but the LTPS TFT has some problems such as uniformity and high cost for large-area displays.[4−6] For that reason, there is increasing interest in utilizing the amorphous silicon (a-Si) TFT and oxide TFT backplanes for the large area AMOLEDs.[7−10] Since a-Si TFT and oxide TFT backplanes mainly have n-type transistor characteristics, the inverted OLED structure with the bottom cathode is more advantageous than the conventional OLED structure with the bottom anode. For instance, when the conventional OLED structure is used with an n-type transistor, a voltage drop happens because the anode of the OLED is connected to the source electrode of the TFT, causing image sticking in the AMOLED display.[11] On the other hand, the voltage drop is minimized in the inverted OLED structure because the bottom cathode of the inverted OLED can be directly connected to the drain line of the n-type TFT.

Efficient electron injection is an important issue in the inverted bottom-emission OLEDs (IBOLEDs) because there are few proper cathode materials for the device. Indium tin oxide (ITO) is usually used as a cathode in the IBOLEDs because of its high optical transparency and electrical conductivity, but ITO has a high work function of 4.8 eV, which can limit electron injection from ITO to an electron transporting layer (ETL) of IBOLEDs. In order to improve the electron injection from the ITO cathode, various methods have been reported such as an insertion of thin metallic layers with low work functions[12] and use of n-type doped ETLs using lithium (Li),[13] cesium (Cs) compound,[14−16] and rubidium (Rb) compound.[17] However, such methods can lead to operational instability by oxidation of metal or diffusion of metal dopants.[18,19] Also, those methods need a vacuum process which makes the manufacturing costs increase. In this respect,

Received: November 20, 2012
Accepted: February 22, 2013
Published: February 22, 2013

electron injection layers (EILs) using solution processes are very attractive. Various solution processable EILs have been reported such as conjugated polymer[20] and n-type metal oxides[21−23] such as zinc oxide (ZnO),[24,25] titanium dioxide (TiO_2),[26] and zirconium dioxide (ZrO_2).[27] However, most n-type metal oxides using the precursor based sol−gel method require high annealing temperature over 300 °C for better electron transport properties; the substrate and prior layers have to endure the process temperature. Recently, n-type colloidal nanoparticles (NPs) such as ZnO NPs are widely used as an EIL in the optoelectronic devices.[28−33] They have good optical and electrical properties and need low process temperature below 100 °C, but ZnO are unstable under UV illumination as reported previously.[34] Therefore, we introduce tin dioxide (SnO_2) NPs instead of ZnO as an EIL which has a wide band gap and low sensitivity to UV degradation compared to ZnO.[34,35] They also have good electron transporting properties and low work function, so that they can be utilized as an efficient and transparent EIL for OLEDs. There are a few reports on light-emitting devices using the sputtered SnO_2 layer as the EIL which results in significant exciton quenching,[36] whereas studies reporting SnO_2 NPs as a charge transport layer have not been established yet.

In this paper, green phosphorescent dye based efficient IBOLEDs using SnO_2 NPs as an EIL are introduced. They showed significantly improved performances compared to the devices without SnO_2 NPs, particularly in terms of the efficiency and driving voltage. Moreover, the deposition process of SnO_2 NPs needs much lower temperature (100 °C to remove the residual solvent) compared to the methods based on metal oxide precursors, so that it can also be applicable to the flexible devices with a plastic substrate.

EXPERIMENTAL SECTION

Measurements. The thickness and roughness of the SnO_2 NP films on ITO were measured using an ellipsometer and an atomic-force microscope (AFM), respectively, according to the concentration of SnO_2 NP solution. The optical absorption and crystallinity of the SnO_2 NP film were observed using an UV−vis spectrophotometer and X-ray diffraction (XRD) technique. The energy levels of ITO and SnO_2 film were measured by ultraviolet photoemission spectroscopy (UPS). The energy levels of the other organic materials, except 3TPYMB whose values are reported in the previous paper,[37] were measured by an AC-2 photoelectron spectrometer (RKI Instruments). The current−voltage characteristics were measured using a source−measurement unit, and the luminance and efficiencies were calculated from photocurrent measurement data obtained with a calibrated Si photodiode. The EL spectra were obtained using a spectroradiometer. For measuring the angular dependence of irradiance and emission spectra, an optical fiber, a monochromator combined with a photomultiplier tube detector, and a rotation stage were used.

Device Fabrication. We fabricated the OLEDs on ITO-coated glass substrates after cleaning and drying them thoroughly. After the UV−ozone treatment, SnO_2 NPs dispersed in water (H_2O) were spin-coated with a spin speed of 2000 rpm for 60 s and then dried in the oven filled with nitrogen gas at 100 °C for an hour to remove the residual solvent. The SnO_2 NPs were used as purchased from a commercial company (MKnano). On the top of the SnO_2 NP layer, the other layers were deposited in succession by the vacuum thermal evaporation. Figure 1 shows the structure of inverted bottom-emission green phosphorescent OLED along with a schematic energy level diagram, consisting of ITO/SnO_2 (x wt %) where x = 0.5, 1.0, 1.5, and 3.0/tris[3-(3-pyridyl)mesityl]borane (3TPYMB) (40 nm) as an ETL/fac-tris(2-phenylpyridinato-*N*,C2′)iridium(III) ($Ir(ppy)_3$) doped 4,4′-*N*,*N*′-dicarbazolbiphenyl (CBP) with the doping ratio of 8 wt % as a green-emitting layer (30 nm)/1,1-bis[(di-4-tolylamino)phenyl]-

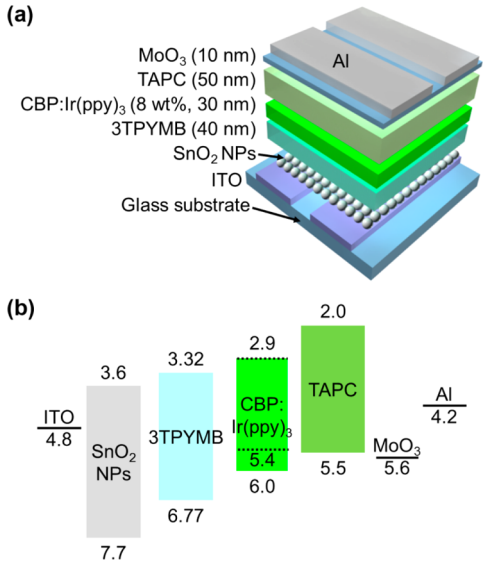

Figure 1. (a) Device structure and (b) schematic energy level diagram of the inverted bottom-emission green phosphorescent OLEDs with SnO_2 NPs as an electron injection layer.

cyclohexane (TAPC) (50 nm) as a hole transporting layer (HTL)/molybdenum trioxide (MoO_3) as a hole injection layer (HIL) (10 nm)/Al (100 nm) as an anode. All organic materials were used as purchased from commercial companies.

RESULTS AND DISCUSSION

The size of SnO_2 NPs was about 5 nm measured by the transmission electron microscopy (TEM) image as shown in Figure S1 in Supporting Information. The thickness of the SnO_2 NP layers spin-coated from 1.0, 1.5, and 3.0 wt % solutions were 15, 17, and 27 nm, respectively. The thickness of the SnO_2 NP layer with 0.5 wt % solution was too thin to be measured accurately with an ellipsometer. Figure 2 shows the AFM images of the SnO_2 NP films formed with different concentrations on the ITO substrates. The root-mean-square (RMS) roughness of the SnO_2 NP layers spin-coated from 0.5, 1.0, 1.5, and 3.0 wt % solutions are 3.40, 3.26, 2.94, and 2.78 nm, respectively. The RMS roughness of the SnO_2 films was much smoother than that of ITO (4.20 nm), and it was slightly decreased as the concentration of SnO_2 NPs increased. The UV−vis absorption spectrum of the SnO_2 NP film shows that the film is highly transparent over the entire visible spectral region with the absorption edge of around 300 nm (see Figure S2, Supporting Information). Also, owing to the low temperature thermal treatment (at 100 °C), the SnO_2 NP film retained the amorphous state as shown in the XRD patterns in Figure S3, Supporting Information. These results indicate that the SnO_2 NP layer can be used as a functional layer at the interface between ITO and the ETL of OLEDs.

Figure 3 shows the current density−voltage (J−V) and luminance−voltage (L−V) characteristics of the devices with different SnO_2 NPs concentrations as well as the control device without SnO_2 NPs. It is clear that the current density and luminance of the devices increased significantly by inserting the SnO_2 NP layer compared to the control device without the SnO_2 NP layer. In case of the device with 1.5 wt % SnO_2 NPs, for example, the maximum luminance was 27 575 cd/m^2 and the driving voltage for the luminance of 1000 cd/m^2 was 17.1 V, whereas those values were 2512 cd/m^2 and 24.0 V,

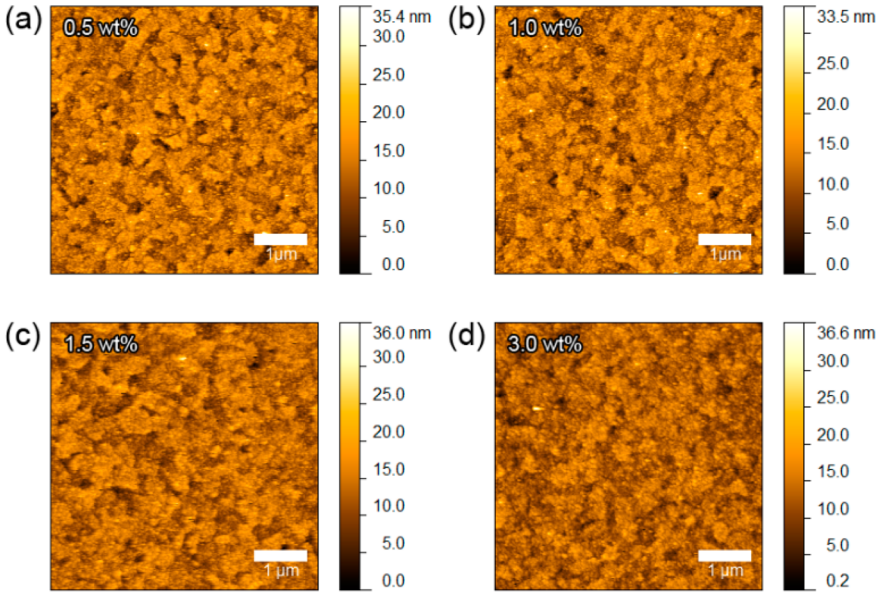

Figure 2. AFM images ($5 \times 5\ \mu m^2$) of SnO_2 NP films with different concentrations of (a) 0.5 wt %, (b) 1.0 wt %, (c) 1.5 wt %, and (d) 3.0 wt %.

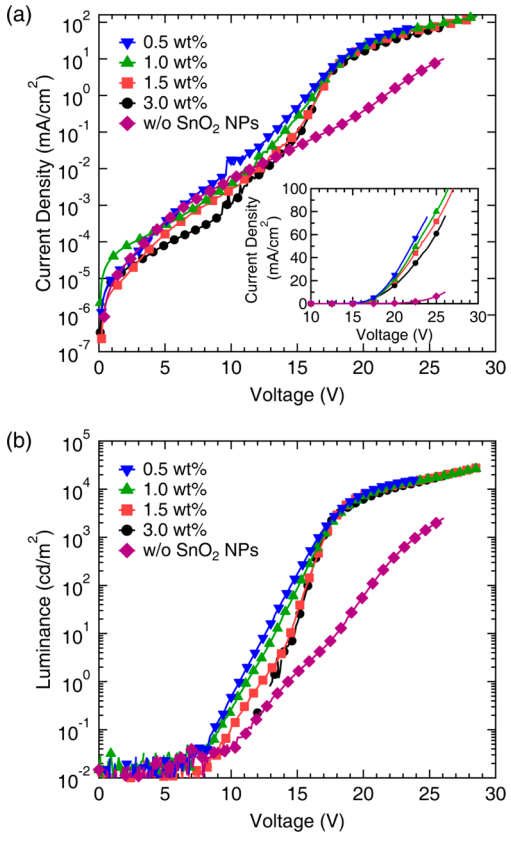

Figure 3. (a) Current density–voltage (inset in linear scale) and (b) luminance–voltage characteristics of the devices with different SnO_2 NPs concentrations.

respectively, for the device without the SnO_2 NP layer. This result indicates that the insertion of the SnO_2 NP layer makes the electron injection more efficient through the improved energy level matching at the interface between ITO and 3TPYMB. As depicted in Figure 1b, the electron injection barrier from ITO to 3TPYMB is 1.48 eV, and it is reduced to 1.2 eV using the SnO_2 layer. The current density and luminance at the same voltage slightly decreases as the concentration of SnO_2 NPs increases because the total thickness (or resistance) of the device increases. The turn-on voltage is also decreased by inserting the SnO_2 layer and shows the similar trend depending on the concentration of SnO_2 NPs, although it is quite high because still there is a large electron injection barrier of over 1 eV. Compared with ZnO NPs as an EIL in the previous report,[31] the devices with SnO_2 NPs have higher driving voltage due to the larger energy barrier between the ITO and SnO_2 layer. Nonetheless, the use of SnO_2 NPs in an optoelectronic device is meaningful for other applications owing to the advantages of solution processability at low temperature, surface roughness, and photostability as described above.

Figure 4a shows that the devices with the SnO_2 NP layers exhibit much higher external quantum efficiencies (EQEs) compared with that of the device without the SnO_2 NP layer. The device with the 3.0 wt % SnO_2 NPs shows the highest efficiencies of 15.6% in EQE or 51.1 cd/A in luminous current efficiency (LCE) at 1000 cd/m^2, which is about two times higher than that of the device without the SnO_2 NP layer. As more electrons are injected to the ETL in the devices with the SnO_2 NP layer, electron–hole balance is enhanced and thus the EQEs are higher than that of the control device. The LCE and driving voltage at the luminance of 1000 cd/m^2 as a function of SnO_2 NPs concentrations are plotted in Figure 4b. Comparing the performances of the IBOLEDs with different SnO_2 layer thicknesses, a higher efficiency was obtained in the device with a thicker SnO_2 film. It is attributed to the surface morphology of the SnO_2 film which was getting smother in the thicker film. The performances in terms of driving voltage for 1000 cd/m^2, the maximum luminance, EQE, LCE, and luminous power efficiency (LPE) along with the thickness of SnO_2 layer are summarized in Table 1.

Figure 5a shows the EL spectra, normalized at the main emission peak (~512 nm), for the IBOLEDs with and without the SnO_2 NP layer measured at the current density of 5.1 mA/cm^2. They have a typical spectral shape originating from $Ir(ppy)_3$, and all the EL spectra are in the same shape regardless of the existence and thickness of SnO_2 NPs. This means that the SnO_2 NP layer scarcely affects the EL spectra of the

dx.doi.org/10.1021/am302787y | ACS Appl. Mater. Interfaces 2013, 5, 1977–1981

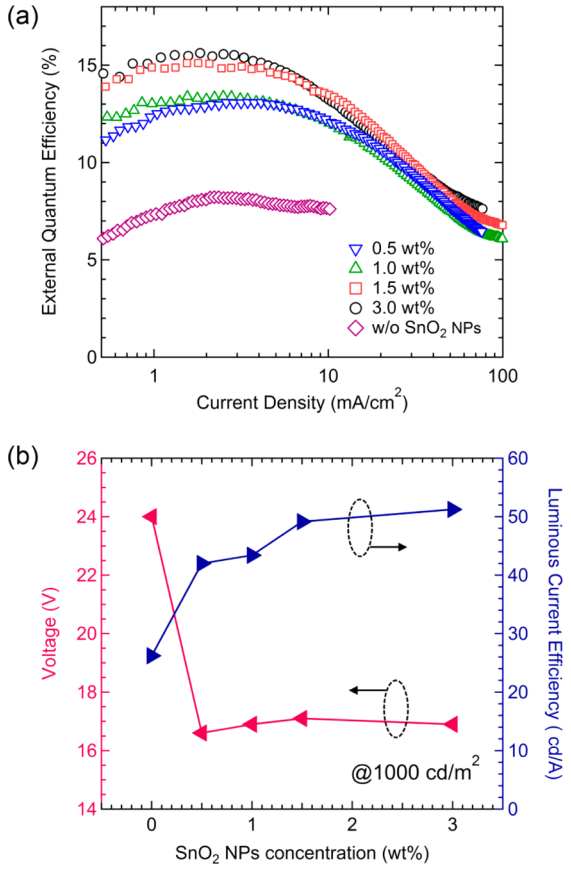

Figure 4. (a) External quantum efficiency−current density characteristics of the devices with different SnO_2 NPs concentrations. (b) The luminous current efficiency and driving voltage at 1000 cd/m^2 as a function of SnO_2 NPs concentrations.

Table 1. Summary of the Device Performances with Different Thicknesses of SnO_2 Layer

SnO_2 concentration	roughness (nm)	V_{1000}[a] (V)	luminance[b] (cd/m^2)	EQE[b] (%)	LCE[b] (cd/A)	LPE[b] (lm/W)
w/o SnO_2	4.20 (ITO)	24.0	2512	8.2	26.6	3.6
0.5 wt %	3.40	16.6	15843	13.1	42.4	8.1
1.0 wt %	3.26	16.9	27062	13.4	43.5	8.3
1.5 wt %	2.94	17.1	27575	15.1	49.3	9.2
3.0 wt %	2.78	16.9	19115	15.6	51.1	9.6

[a]The driving voltage for the luminance of 1000 cd/m^2. [b]The maximum values.

IBOLEDs (e.g., absorption or scattering) because the layer is highly transparent and amorphous as confirmed above. Figure 5b,c shows the angular dependence of irradiance and EL spectra of the device with the SnO_2 NP layer (1.5 wt %), respectively. The angular irradiance characteristic shows that the IBOLED with the SnO_2 NP layer has nearly Lambertian emission profile. In addition, the EL spectra at different viewing angles also changed little from the normal direction to 80° off the normal direction; the main emission peaks were kept in almost the same position while the intensity of the shoulder peaks around 540 nm were changed slightly. Maintaining the emission colors depending on the viewing angle is one of the important requisites for the application of OLEDs to display devices. Consequently, we believe that adopting SnO_2 NPs as

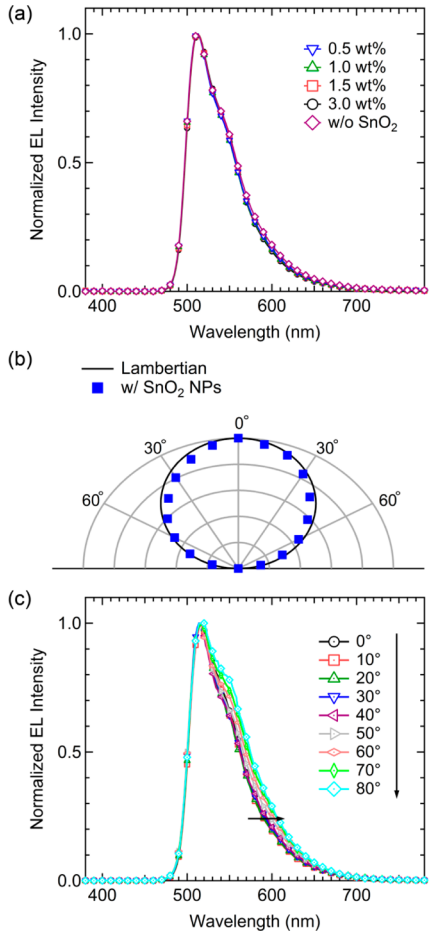

Figure 5. (a) Normalized EL spectra of the devices with different SnO_2 NPs concentrations at the current density of 5.1 mA/cm^2. (b) Angular distribution of the irradiance (normalized to the 0° irradiance) and (c) normalized EL spectra of the IBOLED with 1.5 wt % SnO_2 NPs with different measuring angles.

the EIL in the IBOLEDs is meaningful, a lot in terms of the potential for future displays as well as the device performances.

CONCLUSION

We have demonstrated a highly efficient inverted bottom-emission green phosphorescent OLED with outstanding angular emission characteristics using the SnO_2 NP layer as an EIL. Since SnO_2 NPs possess a wide band gap, low work function, and low temperature processability, they can be utilized as an effective electron injection layer with high transparency. The devices with the SnO_2 NP layer exhibited much higher efficiency and lower driving voltage compared to the device without the SnO_2 NP layer owing to the improved energy level alignment. In addition, the emission pattern of the IBOLED with the SnO_2 NP layer was close to the ideal Lambertian pattern, and few EL spectrum shifts were observed as the viewing angle changed. Owing to these advantages of the use of SnO_2 NPs in the EIL, the IBOLEDs can be applicable for future display devices. We also think SnO_2 NPs can be used for various optoelectronic devices such as organic photovoltaic cells and colloidal quantum-dot based light-emitting diodes as well as OLEDs.

■ ASSOCIATED CONTENT

Supporting Information

TEM image of SnO_2 NPs, UV−vis absorption spectrum, and XRD data of the SnO_2 NP film. This information is available free of charge via the Internet at http://pubs.acs.org/.

■ AUTHOR INFORMATION

Corresponding Author

*E-mail: jkwak@dau.ac.kr (J.K.); chlee7@snu.ac.kr (C.L.).

Present Address

[§]Components & Materials Research Laboratory, Electronics and Telecommunications Research Institute (ETRI), Daejeon 305-700, Republic of Korea.

Notes

The authors declare no competing financial interest.

■ ACKNOWLEDGMENTS

This work was supported by the Industrial strategic technology development program (10041556, Material and device development of common and emissive layer with under 4 V driving voltage and over 50 000 h lifetime characteristics for 50 in. class AMOLED TV applications) funded by the Ministry of Knowledge Economy (MKE) of Korea. We also appreciate the financial support from the National Research Foundation of Korea (NRF) through the BK21 Program and the Basic Science Research Program (2011-0022716) grant funded by the Ministry of Education, Science and Technology (MEST) of Korea.

■ REFERENCES

(1) Han, C.-W.; Kim, K.-M.; Bae, S.-J.; Choi, H.-S.; Lee, J.-M.; Kim, T.-S.; Tak, Y.-H.; Cha, S.-Y.; Ahn, B.-C. *SID Int. Symp. Dig. Tech. Pap.* **2012**, *43*, 279−281.

(2) Reineke, R.; Lindner, F.; Schwartz, G.; Seidler, N.; Walzer, K.; Lüssem, B.; Leo, K. *Nature* **2009**, *459*, 234−238.

(3) Yamae, K.; Tsuji, H.; Kittichungchit, V.; Matsuhisa, Y.; Hayashi, S.; Ide, N.; Komoda, Y. *SID Int. Symp. Dig. Tech. Pap.* **2012**, *43*, 694−697.

(4) Stewart, M.; Howell, R. S.; Pires, L.; Hatalis, M. K. *IEEE Trans. Electron Devices* **2001**, *48*, 845−851.

(5) Lih, J.-J.; Sung, C.-F.; Li, C.-H.; Hsiao, T.-H.; Lee, H.-H. *SID Int. Symp. Dig. Tech. Pap.* **2004**, *35*, 1504−1507.

(6) Lee, I.; Im, C.; Kim, Y.; Kwon, D.; Kim, J.; Ko, M.; Yun, J.; Yeo, J.; Im, J.; Kim, S. *SID Int. Symp. Dig. Tech. Pap.* **2011**, *42*, 101−103.

(7) He, Y.; Hattori, R.; Kanicki, J. *IEEE Trans. Electron Devices* **2001**, *48*, 1322−1325.

(8) Nathan, A.; Alexander, S.; Servati, P.; Sakariya, K.; Striakhilev, D.; Huang, R.; Kumar, A.; Church, C.; Wzorek, J.; Arsenault, P. *SID Int. Symp. Dig. Tech. Pap.* **2005**, *36*, 320−323.

(9) Shih, T.-H.; Tsai, T.-T.; Chen, K.-C.; Lee, Y.-C.; Fang, S.-W.; Lee, J.-Y.; Hsieh, W.-J.; Tseng, S.-H.; Chiang, Y.-M.; Wu, W.-H.; Wang, S.-C.; Lu, H.-H.; Chang, L.-H.; Tsai, L.; Chen, C.-Y.; Lin, Y.-H. *SID Int. Symp. Dig. Tech. Pap.* **2012**, *43*, 92−94.

(10) Semenza, P. *Inf. Disp.* **2012**, *28*, 14−16.

(11) Hsieh, H.-H.; Tsai, T.-T.; Chang, C.-Y.; Wang, H.-H.; Huang, J.-Y.; Hsu, S.-F.; Wu, Y.-C.; Tsai, T.-C.; Chuang, C.-S.; Chang, L.-H.; Lin, Y.-H. *SID Int. Symp. Dig. Tech. Pap.* **2010**, *41*, 140−143.

(12) Chu, T.-Y.; Chen, J.-F.; Chen, C. H. *Jpn. J. Appl. Phys.* **2006**, *45*, 4948−4950.

(13) Zhou, X.; Pfeiffer, M.; Huang, J. S.; Blochwitz-Nimoth, J.; Qin, D. S.; Werner, A.; Drechsel, J.; Maenning, B.; Leo, K. *Appl. Phys. Lett.* **2002**, *81*, 922−924.

(14) Chu, T.-Y.; Chen, J.-F.; Chen, S.-Y.; Chen, C.-J.; Chen, C. H. *Appl. Phys. Lett.* **2006**, *89*, 053503.

(15) Chen, S.-Y.; Chu, T.-Y.; Chen, J.-F.; Su, C.-Y.; Chen, C. H. *Appl. Phys. Lett.* **2006**, *89*, 053518.

(16) Xiong, T.; Wang, F.; Qiao, X.; Ma, D. *Appl. Phys. Lett.* **2008**, *92*, 263305.

(17) Lee, J.-H.; Wang, P.-S.; Park, H.-D.; Wu, C.-I.; Kim, J.-J. *Org. Electron.* **2011**, *12*, 1763−1767.

(18) D'Andrade, B. W.; Forrest, S. R.; Chwang, A. B. *Appl. Phys. Lett.* **2003**, *83*, 3858−3860.

(19) Parthasarathy, G.; Shen, C.; Kahn, A.; Forrest, S. R. *J. Appl. Phys.* **2001**, *89*, 4986−4992.

(20) Zhong, C.; Liu, S.; Huang, F.; Wu, H.; Cao, Y. *Chem. Mater.* **2011**, *23*, 4870−4876.

(21) Sessolo, M.; Bolink, H. J. *Adv. Mater.* **2011**, *23*, 1829−1845.

(22) Vaynzof, Y.; Kabra, D.; Brenner, T. J. K.; Sirringhaus, H.; Friend, R. H. *Isr. J. Chem.* **2012**, *52*, 496−517.

(23) Panthani, M. G.; Korgel, B. A. *Annu. Rev. Chem. Eng.* **2012**, *3*, 287−311.

(24) Kabra, D.; Lu, L. P.; Song, M. H.; Snaith, H. J.; Friend, R. H. *Adv. Mater.* **2010**, *22*, 3194−3198.

(25) Ryan, J. W.; Palomares, E.; Martínez-Ferrero, E. *J. Mater. Chem.* **2011**, *21*, 4774−4777.

(26) Bolink, H. J.; Coronado, E.; Repetto, D.; Sessolo, M.; Barea, E. M.; Bisquert, J.; Garcia-Belmonte, G.; Prochazka, J.; Kavan, L. *Adv. Funct. Mater.* **2008**, *18*, 145−150.

(27) Tokmoldin, N.; Griffiths, N.; Bradley, D. D. C.; Haque, S. A. *Adv. Mater.* **2009**, *21*, 3475−3478.

(28) Chiba, T.; Pu, Y.-J.; Hirasawa, M.; Masuhara, A.; Sasabe, H.; Kido, J. *ACS Appl. Mater. Interfaces* **2012**, *4*, 6104−6108.

(29) Chiba, T.; Pu, Y.-J.; Sasabe, H.; Kido, J.; Yang, Y. *J. Mater. Chem.* **2012**, *22*, 22769−22773.

(30) Ryu, S. Y.; Kim, S. H.; Kim, C. S.; Jo, S.; Lee, J. Y. *Curr. Appl. Phys.* **2012**, *12*, 1378−1380.

(31) Lee, H.; Park, I.; Kwak, J.; Yoon, D. Y.; Lee, C. *Appl. Phys. Lett.* **2010**, *96*, 153306.

(32) Qian, L.; Zheng, Y.; Choudhury, K. R.; Bera, D.; So, F.; Xue, J.; Holloway, P. H. *Nano Today* **2010**, *5*, 384−389.

(33) Kwak, J.; Bae, W. K.; Lee, D.; Park, I.; Lim, J.; Park, M.; Cho, H.; Woo, H.; Yoon, D. Y.; Char, K.; Lee, S.; Lee, C. *Nano Lett.* **2012**, *12*, 2362−2366.

(34) Kuwabara, T.; Tamai, C.; Omura, Y.; Yamaguchi, T.; Taima, T.; Takahashi, K. *Org. Electron.* **2013**, *14*, 649−656.

(35) Kay, A.; Grätzel, M. *Chem. Mater.* **2002**, *14*, 2930−2935.

(36) Caruge, J. M.; Halpert, J. E.; Wood, V.; Bulović, V.; Bawendi, M. G. *Nat. Photon.* **2008**, *2*, 247−250.

(37) Tanaka, D.; Takeda, T.; Chiba, T.; Watanabe, S.; Kido, J. *Chem. Lett.* **2007**, *36*, 262−263.